RESEARCH ARTICLE OPEN ACCESS

First Principle Study of Thermoelectric Properties of SnSb Alloy

Sangay Wangdi*, Sonam Dendup**,Sonam Dorji***
*(Physics Department, Peljorling Higher Secondary School, Tashicholing, Samtse:BHUTAN.
Email: sangaywangdi@education.gov.bt)
** (Physics Department, Shaba Higher Secondary School, Paro: BHUTAN
*** (Physics Department, Kidheykhar Higher Secondary School, Mongar: BHUTAN

----------**********----------

Abstract:

In this study we have performed first principle calculations to study the electronic and its resulting thermoelectric properties of SnSb alloy within the framework of density functional theory (DFT). Generalized Gradient Approximation (GGA) is employed to model the exchange and correlation of Kohn-Sham Eigen states. The DOS for SnSb around Fermi level is about 1.2 states/eV. From the band structure it is observed that there is no electronic band gap for SnSb at Fermi level which indicates the metallic behavior of SnSb. The thermoelectric properties of SnSb are calculated using BoltzTraP code based on semi-classical Boltzmann transport equations. The calculated value of zT of SnSb is 0.48 at 200 K.

Keywords —Tin Antimony, Quantum ESPRESSO, Density functional theory (DFT), GGA,Boltzmann transport equations (BTE)

----------**********----------

1. INTRODUCTION

Thermoelectric research has witnessed groundbreaking progress over past 20-25 years due to exciting Physics and Chemistry that underlies the realization of high-performance thermoelectric materials [1]. High-efficiency thermoelectric (TE) materials are important for power generation devices that are designed to convert waste heat into electrical energy [2]. They are also used in solid-state refrigerator devices [3]. The conversion of waste heat into electrical energy plays an important role in our current challenge to develop alternative energy technologies to reduce our dependence on fossil fuels and ultimately reduce greenhouse gas emissions [1-3]. The conversion efficiency of the thermoelectric material is controlled by a dimensionless parameter called the Figure of Merit (zT) [4] given as$zT = \frac{S^2\sigma T}{\kappa}$, where$S$ is the Seebeck coefficient, σ the electrical conductivity, κ the thermal conductivity, and T the absolute temperature. High performance thermoelectric materials are usually considered to have zT at least equal to or greater than one [5]. In order to obtain higher zT value, as evident from the equation above, the thermoelectric material should have higher Seebeck coefficient (SC), higher electrical conductivity (σ) and lower thermal conductivity (κ). This study is aimed at checking the thermoelectric properties of SnSb by first principle calculations within the framework of density functional theory (DFT). The thermoelectric properties are calculated solving the Boltzmann transport equations (BTE).

This document is a template. An electronic copy can bedownloaded from the conference website. For questions onpaper guidelines, please contact the conference publicationscommittee as indicated on the conference website. Information about final paper submission is available from the conference website.

2. COMPUTATIONAL DETAILS

This study focuses on the computation of structural, electronic and thermoelectric properties of SnSb by employing the plane wave basis set generated by ultrasoft pseudopotential using Rappe-Rabe-Kaxiras-Joannopoulos (RRKJ) [6] method within density functional theory (DFT) formalism using Quantum ESPRESSO package [7]. According to Shrivastava et al. the crystal structure of SnSb alloy is found to exist most stable in NaCl-type structure whose crystal structure is cubic with *fcc* lattice type. It is found under space group of *Fm-3m (225)* [3-6]. The starting model of SnSb is generated with Sn at atomic site (0.0, 0.0, 0.0) and Sb at (0.5 ,0.5, 0.5). The cubic structure of SnSb is generated using VESTA. The ground state calculations are carried out by the DFT code Quantum ESPRESSO [8]. The exchange-correlation functional was approximated by generalized gradient approximation (GGA) as defined by Perdew-Burke-Ernzerhof (PBE) [9].
The structure has been relaxed by varying the kinetic energy cut off for plane wave basis set, *k*-points mesh density, degauss and lattice cell constant for the least possible value of total energy. To achieve excellent convergence, the kinetic energy cut off of 40 Ry has been selected for the expansion of plane wave basis set. Monkhorst and Pack [10] matrix of 6 x 6 x 6 *k*-points were used for the self-consistent field (scf) calculation. However, a denser grid of 12 x 12 x 12 *k*-points has been used for meshing the Brillouin zone (BZ) to compute structural, electronic and thermoelectric properties. The value of degauss has been selected to be 0.02Ry.The thermoelectric properties of SnSb have been computed using BoltzTraP code which is based on semi-classical Boltzmann transport equations (BTE) [11].

3. Result and Discussion

3.1. Geometry Optimization

The valence electron configuration chosen by an ultrasoft pseudo potential (USPP) for Sn and Sb atoms is *5s* and *5p*. All the discussions are based on the results of fully optimized geometry. The following optimizations were carried out;

3.1.1. Kinetic energy cut-off (*ecutwfc*) optimization

The kinetic energy cut-off (*ecutwfc*) optimization was done to limit the number of plane waves with energy smaller than or equal to kinetic energy cut-off.In this study, the *ecutwfc* value converged at 40 Ry which when varied in the range of 10-80 Ry as shown in the Figure below.

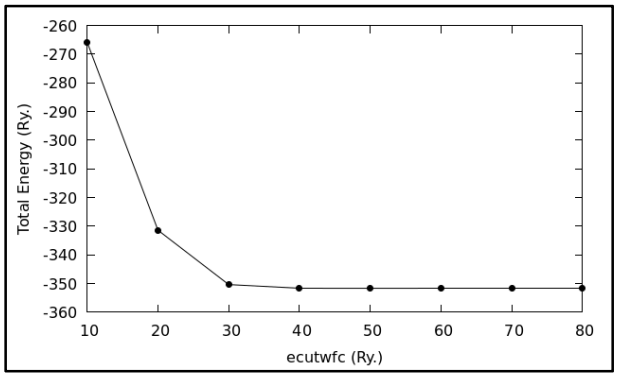

Figure 1: Kinetic energy cut off optimization of SnSb

3.1.2. k-point optimization

The total energy and density calculations ideally are carried out for all values of k plane waves. However, we practically limit only for a finite number of k plane waves. The summation in limited Brillouin Zone (BZ) sampling was adapted where we used Monkhorst-Pack mesh variation from $2 \times 2 \times 2$ to $12 \times 12 \times 12$ for finding the best convergence and total energy value as shown below.

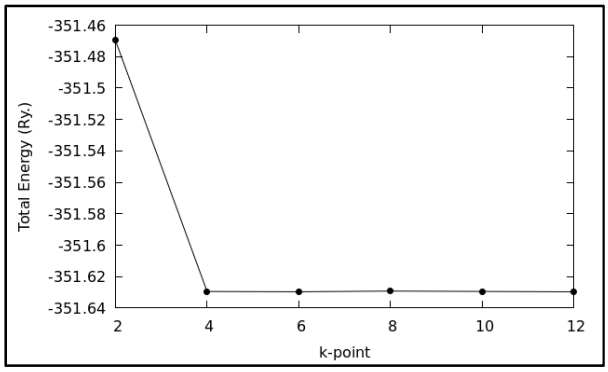

Figure 2: k-point optimization of SnSb

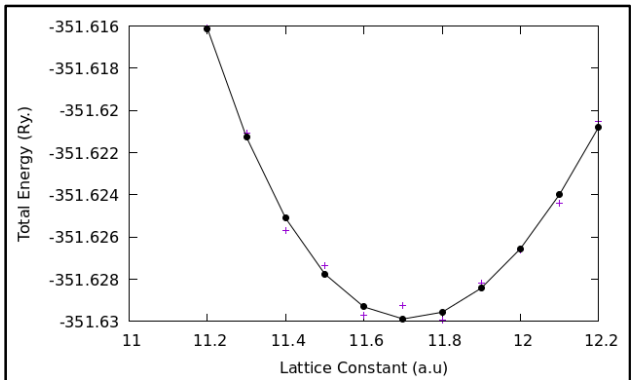

Figure 3: Lattice parameter optimization of SnSb

3.1.3. Lattice constant optimization

Structural optimization was done by optimizing the lattice constant. The total energies which are calculated as a function of lattice parameter are fitted to Murnaghan's equation of state [12] in order to obtain equilibrium lattice constant, volume and bulk modulus as stated below:

$$E(V) = E_0 + \frac{9BV_0}{16} \times \left\{ \left[\left(\frac{V_0}{V}\right)^{\frac{2}{3}} - 1 \right]^3 B' + \left[\left(\frac{V_0}{V}\right)^{\frac{2}{3}} - 1 \right]^2 \left[6 - 4 \left(\frac{V_0}{V}\right)^{\frac{2}{3}} \right] \right\}$$

where E_0 is minimum energy, V_0 is optimized volume, V is deformed volume. P is the pressure,B is the bulk modulus and B' is the pressure derivative of the bulk modulus given by:

$$P = \frac{dE}{dV}, \quad B = V\frac{dP}{dV} = \frac{d^2E}{dV^2}, \qquad B' = \frac{dB}{dP}.$$

The optimum value of calculated lattice constant of SnSb is 11.7127 Bohr against its experimental value of 11. 5122 Bohr as reported by P .V. Sreenivasa Reddy and V. Kanchana in [13]. The calculated value of bulk modulus is 49.2 GPa. Similarly, the calculated value of volume is $401.71(\text{a. u})^3$. There are some other data as report in [14] and [15]. The difference in the values of calculated parameters with the data reported in other theories as shown in table 1 is attributed for the fact that LDA is used in other theories which might either have underestimated the values of parameters or overestimated with GGA. The converged value of equilibrium lattice constant, volume and bulk modulus are tabulated in Table 1.

Table 1: Equilibrium value of lattice constant of SnSb in comparison with experimental value and other theoretical values in NaCl-type structure

Parameter	GGA	Expt.	Other theory
a (a. u)	11.7127	11.5122 [3]	11.6798 ,11.4139 [4], 11.4328, 11.6652 [3]
Volume $(\text{a. u})^3$	401.71	-	387.2 [3]
Bulk Modulus (GPa)	49.2	-	52.7,53.1 [4], 63 [3]

3.2.Structural Property

As reported by Deepika Shrivastava et al (2016), SnSb is found to crystallize into cubic rock salt

(NaCl-type) structure at ambient conditions. During the investigation of crystal structure of SnSb, it is found to give excellent X-ray powder photograph of the well-known pattern common to sodium chloride structures [12-15]. Further, Valery Pierre Vasil'ev as reported in [16] ascertained that at 1:1 ratio of Sn and Sb, SnSb assumes the perfect structure rock salt structure. Therefore, for the purpose of this study the structure of SnSb is drawn using VESTA software as shown below.

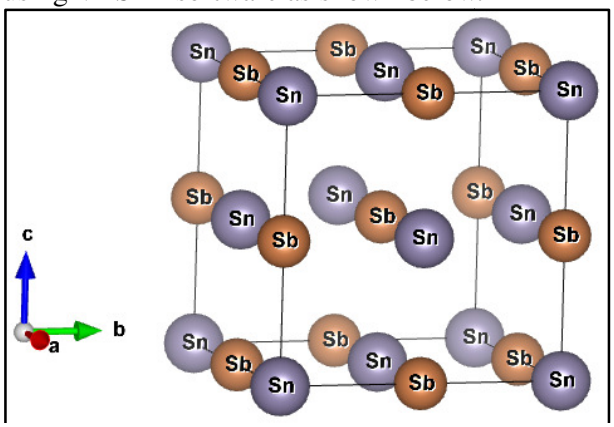

Figure 4: Cubic structure of SnSB generated using VESTA

In the figure above, the structure of SnSb is generated with Sn at atomic site(0.0,0.0,0.0) and Sb at (0.5,0.5,0.5). Thus, the structure generated is cubic with space group *Fm-3m*, space number *225*.

3.3. Electronic Property

To elucidate the electronic properties of SnSb, we have calculated the total density of states (TDOS), projected density of states (PDOS) and band structure of SnSb as shown in Figure 5 and Figure 7 respectively. All the electronic structure calculations are performed at their respective equilibrium lattice parameter. The calculated band structure and orbital projected density of states are presented to clarify the characters of bands.

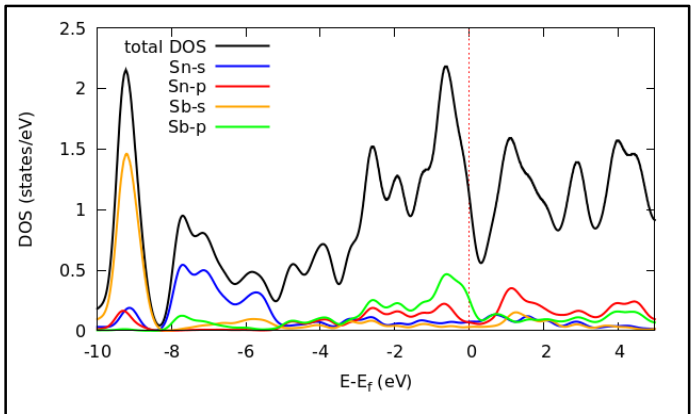

Figure 5: Total and projected DOS of SnSb

From the Figure 5 it is clear that the lowest occupied bands for SnSb is due to '*s*' orbital of Sb producing a sharp peak at about -9.0 eV. The second lowest bands is due to the's' states of Sn. The last two bands below Fermi level are characterized by '*p*' states of Sn and Sb in both the cases. Around Fermi level there is a hybridization of '*p*' and'*s*' states of Sn atom which shoes the mixed behavior wit '*p*' state of Sb giving rise to the peak at 0.5 eV. Sn-*p* and Sb-*p* states show a strong hybridization just below and above the Fermi level as a result of which covalent interaction appears between Sn-Sb atoms. The contribution for DOS after Fermi level are mainly due to '*p*' state of Sn atom. The total DOS calculated for SnSb at Fermi level is about 1.2 states/eV against 0.95 states/eV with LDA in [17].

The band structure (BS) indicates the nature of bonding within atoms and determines the nature of material. High symmetry paths of Γ-X-M-Γ-R-X-M-Rwithin Brillouin zone as generated from XCrySDen were chosen and subsequently the electronic band structure of SnSb has been plotted as shown in Figure 7 below.

From the band structure it confirms that there is no band gap for SnSb at Fermi level. This indicates the metallic behavior of SnSb. The extra band crossing the Fermi level shows SnSb having hole nature due to the band crossing from valence band to conduction band. The band at Γpoint is found to

possess Sb-*p* character and at L point around 1 eV has Sn-*p* character.

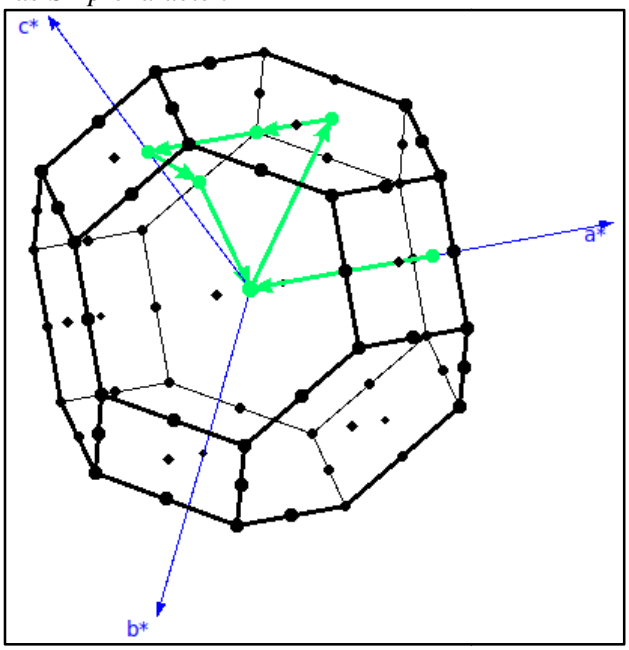

Figure 6: Brillouin zone selection generated using XCrySDen

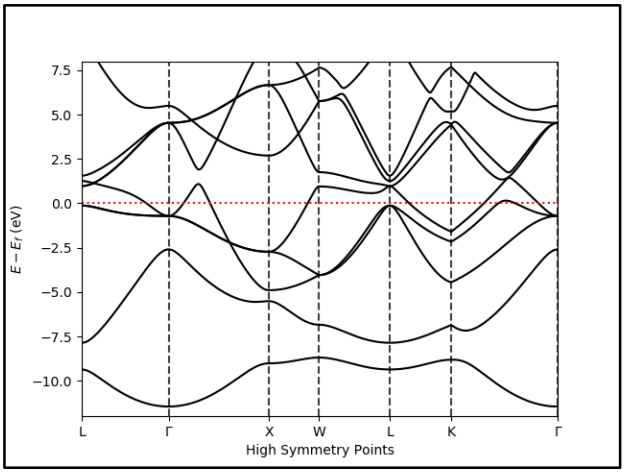

Figure 7: Band structure of SnSb

3.4. Transport Properties

For an efficient TE material, a high value of Seebeck Coefficient (S) and electrical conductivity (σ) with low thermal conductivity (k) is expected [18]. The dimensionless figure of merit can be optimized when these parameters are optimum [19]. To get insight into the TE properties of SnSb, we calculated the S, σ, k, power factor (PF) and figure of merit (zT) using constant relaxation time approximation. Each of these parameters are calculated as a temperature dependence at chemical potential of 0.71663 Ry which is closest to its Fermi energy value 0.71646 Ry.

The value of electrical conductivity divided by relaxation time of SnSb is as shown in the Figure 8 below.

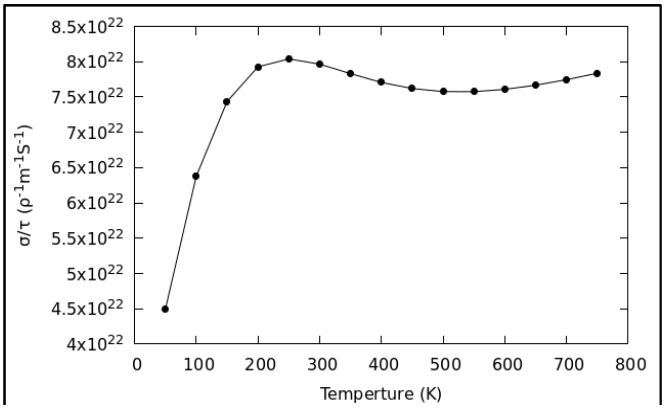

Figure 8: Variation of electrical conductivity of SnSb with temperature

The temperature dependence of σ/τ of SnSb is calculated from a temperature of 50 K to 800 K. The electrical conductivity of SnSb at constant relaxation time increases from 50 K and attains its maximum value of $8 \times 10^{22} \rho^{-1} m^{-1} s^{-1}$ at 250 K. This increase in electrical conductivity from temperature range of 50 K to 250 K shows the behavior of SnSb as semiconducting material as reported by Lakshmi D *et al* (2020) in [20].This is because as the thermal energy increases, the covalent bonds between Sn and Sb atoms as discussed under band structure are broken and more number of charge carriers gain sufficient energy to promote themselves to conduction band from valence band. However, beyond 250 K the mobility fall is more rapid than the rise of charge carrier, and hence the electrical conductivity starts decreasing till 500 K. The electrical conductivity curve remains flat from 500 K onwards signifying the saturation of its conductivity value in the higher temperature region. Hence, for this material, the electrical conductivity makes significant contribution towards

qualifying SnSb as a thermoelectric material at 250 K of temperature.

Figure 9 below shows the variation of Seebeck coefficient (S) of SnSb with temperature. Seebeck coefficient is an essential parameter that is measured to identify the potential thermoelectric performance of a material [21]. By applying a temperature gradient ΔT in a TE couple, consisting of *n*-type and *p*-type materials, the charge carriers diffuse from the hot to the cold side producing and electric potential ΔV. This is known as Seebeck effect. The ratio of the produced voltage to the temperature difference is the thermopower or Seebeck coefficient; $S = \frac{\Delta V}{\Delta T}$

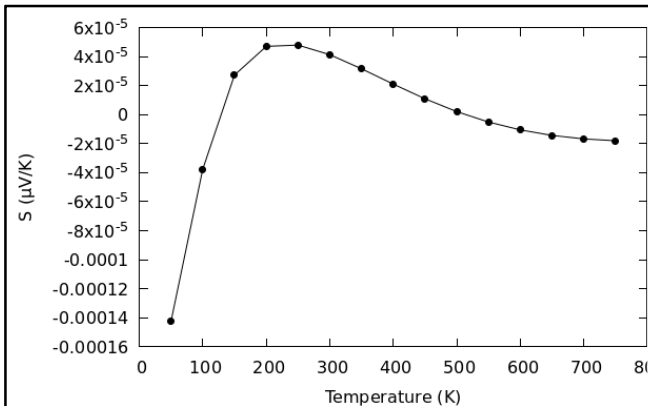

Figure 9: Variation of Seebeck coefficient of SnSb with temperature

In materials where dominant charge carriers are holes, (*p*-type), the Seebeck coefficient has a positive sign, while those dominated by electrons (*n*-type) have negative Seebeck coefficients.
Here, theSeebeck coefficient of SnSb is observed increasing with increasing temperature. The maximum value of SC is about $4 \times 10^{-5} \mu V/K$ at 200K. The maximum peak of S is positive indicating the hole nature dominating in SnSb as discussed under section 4.3 for band structure of SnSb. The positive Seebeck coefficient which is also called as thermo power is expected in the metallic systems if the energy of the conduction band edge increases with temperature and if this effect overcompensates the influence of the energy dependent conductivity, σ (E) [22]. Therefore, the positive S of SnSb is caused due to band edge shift with temperature as shown in Figure 7. However, it is to be noted that the SnSb being a metallic material, its carrier concentration increases with temperature and thus SC decreases slowly beyond 250 K of temperature.

The high values of electrical conductivity (σ) and Seebeck coefficient (SC) contribute to high value of power factor (PF). The plot of PF for SnSb is shown below in Figure 10. Initially at 100 K the value of PF is about $9 \times 10^{13}\ Wm^{-1}K^{-1}s^{-1}$. It decreases from 100 K to 150 K and then again increases till 250 K, after which it decreases linearly and becomes zero at 500 K. The maximum value of PF of SnSb is $1.8 \times 10^{14} Wm^{-1}K^{-1}s^{-1}$ is observed at 250 K.

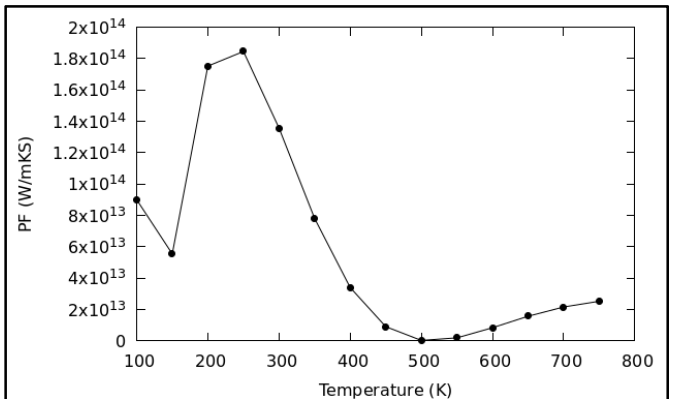

Figure 10: Variation of power factor of SnSb with temperature

The PF value starts increasing again from 500 K. However, PF is maximum value at 250 K for SnSb alloy which correspond to give maximum thermoelectric efficiency of SnSb.

Figure 11 shows the calculated thermal conductivity (κ) of SnSb as a function of temperature. For thermoelectric material to be an efficient one, its thermal conductivity must be relatively less and controlled. The total thermal conductivity consist of two components viz. electronic (k_e) and lattice (k_l) parts.

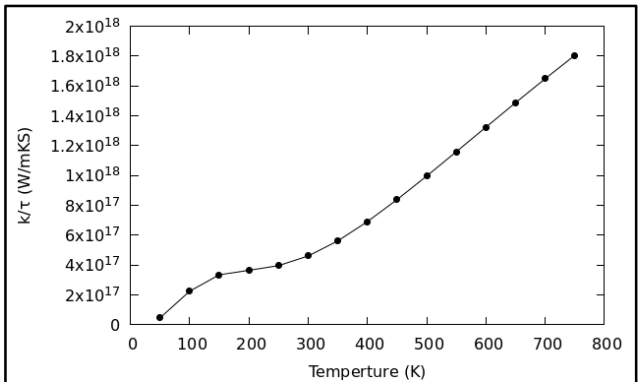

Figure 11: Variation of thermal conductivity of SnSb with temperature

The thermal conductivity increases almost linearly with temperature. At low temperature the electronic part is found dominant over lattice part and thermal conductivity is less. However, with the rise in temperature the lattice thermal conductivity and the overall conductivity increases uniformly. Hence, the thermal conductivity values at higher temperature is not favorable for the purpose of calculating the thermoelectric figure of merit.The figure of merit (zT) for SnSb is shown below in Figure 12.

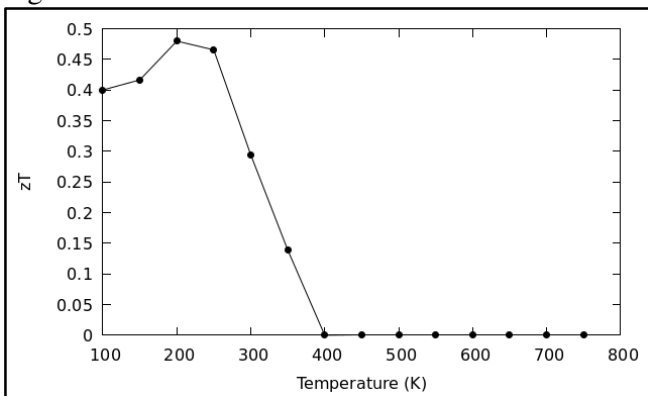

Figure 12: Variation of merit of figure of SnSb with temperature

As discussed, zT value can increase when PF is enhanced while minimizing the κ. In above figure, the value zT is 0.4 at 100 K. It increases from 100 K and its maximum value is obtained at 200 K. After 200 K its value decreases sharply and becomes zero beyond 500 K.

Though the value of zT we reported is lower than the commercialized thermoelectric materials such as $Bi_2Te_3$and $PbTe$[23], it can be enhanced further by means of doping. Here, the observed zT value is 0.48 at 200 K which is comparatively low with commercial thermoelectric materials, mainly due to a high value of κ/τ. The value of κ/τ found is high which is in the order of 10^{17}even at very low temperature, ultimately bringing low value of zT.The value of various transport properties of SnSb is summarized in the Table 2 as shown below;

Table 2: Various transport properties of SnSb

Transport Property	Value	Temperature (K)
Electrical Conductivity ($\rho^{-1}m^{-1}S^{-1}$)	8×10^{22}	250
Seebeck Coefficient ($\mu V/K$)	4×10^{-5}	250
Power Factor (W/mKS)	1.8×10^{14}	250
Thermal Conductivity (W/mKS)	4.7×10^{16}	50
Figure of Merit	0.48	200

4. CONCLUSION

Thermoelectric (TE) materials have gathered immense research interest in the last few decades due to their worth in interconverting heat as well as electricity[24]. Such capability of TE materials can improve fuel efficiency as well as provide a robust alternative energy supply in multiple applications by collecting wasted heat, and therefore assist in finding new energy solutions[25].To construct high-performance TE devices, superior TE materials have to be targeted via various strategies[26]. This is because the development of high-performance TE devices can not only broaden the market for TE applications and but also boost the enthusiasm for TE materialsresearch.

Therefore, in this study we have investigated the thermoelectric properties of SnSb to check its

thermoelectric efficiency. The following are the key results obtained which are consistent with the secondary data available;

1. SnSb is found out to possess cubic structure [3-8] which is most stable in NaCl-type structure with space group *Fm-3m (225)*.
2. SnSb is a metallic material [3, 4] as illustrated through band structure. However, due to strong hybridization between '*p*' states around Fermi level [7-9], covalent bond exist between Sn and Sb atoms [9].
3. From Figure 7 and 9 confirms hole nature of SnSb which strongly agrees with the report by D. Shrivastava et al (2016).
4. The Figure of Merit (zT) of SnSb is found out to 0.48 at 200 K which is less than the values of commercial TE materials reported in [3-10].

Besides the successful study and calculation of thermoelectric properties of SnSb, it can be further studied to enhance the zT of SnSb by exploring various strategies which is beyond the scope of this work. Nevertheless, the present work can form the basis for the other researchers to compare and validate their findings. It should further pave the way to explore this alloy in depth for various device applications.

References

[1] D. Lakshmi, "Compound semiconducting SnSb alloy anode for Li ion batteries: Effect of elemental composition of Sn-Sb," *Semiconductor Science and Technology,* pp. 2-15, 2020, DOI:10.1088/1361-6641/ab708d

[2] Alexander. T. Tesfaye, "The Electrochemical Behavior of SnSb as an Anode for Li-ion Batteries Studied by Electrochemical Impedance Spectroscopy and Electron," *Electrochimica Acta,* vol. 256, no. 155-161, pp. 3-7, 2017.

[3] Chaoli Yin et al "Effect of the synthesis method of SnSb anode materials on their electrochemical properties," *International Journal of Minerals, Metallurgy and Materials,* vol. 32, no. 56, pp. 1-8, 2006.

[4] A. Bulusu. and Greg. Walkar, "Review of electronic transport models for thermoelectric materials," *Superlattices and Microstructures,* vol. 44, no. 1, pp. 3-5, 2008.

[5] D. J.Singh, "Theoretical and computational approaches for identifying and optimizing novel thermoelectric materials," *Semiconductors and Semimetals,* vol. 70, pp. 3-9, 2001.

[6] Hussam Jouhara et al "Waste Heat Recovery Technologies and Applications," *Thermal Science and Engineering Progress,* vol. 6, pp. 1-3, 2018.

[7] D. Enescu, "Thermoelectric Energy Harvesting: Basic Principles and Applications," no. DOI: 10.5772/intechopen.83495, pp. 7-9, 2018.

[8] J. Shuai, "Recent Progress and Future Challenges on Thermoelectric Zintl Materials," in *Department of Physics and TcSUH, University of Houston*, Houston, TX 77204, USA, 2017.

[9] Fang Wang et al., "Technologies and perspectives for achieving carbon neutrality," *The Innovation,* vol. 2, no. 4, pp. 1-3, 2021.

[10] G. Jeffrey Snyder and Alemayouh. H. Snyder, "Figure of Merit ZT of a Thermoelectric Device Defined from Materials," *Energy & Environmental Science,* vol. 4, no. 11 2017, DOI: 10.1039/C7EE02007D

[11] Mario Wolf et al., "High Power Factor vs. High zT—A Review of Thermoelectric Materials for High-Temperature Application," *Entropy,* vol. 21, no. 11 doi:10.3390/e21111058, pp. 1-3, 2019.

[12] W. Kohn et al., "Density Functional Theory of

Electronic Structure," *J. Phys. Chem,* vol. 4, no. 7, pp. 2-6, 1996.

[13] John P. Perdew. a. Stefan. Kurth, "Density Functionals for Non-relativistic Coulomb Systems in the New Century," Department of Physics and Quantum Theory Group, Tulane University,, New Orleans LA 70118, USA, 2003.

[14] N. Harrison, "An Introduction to Density Functional Theory," Department of Chemistry, Imperial College of Science and Medicine, SW7 2AY, London, 2017.

[15] D. G. Truhlar, "Density Functional Theory," Department of Chemistry, University of Minnesota.

[16] N. D. Wood et al., "Computing the Self-Consistent Field in Kohn-Sham Density Functional Theory," *Journal of Physics: Condensed Matter,* vol. 31, no. 45, pp. 11-14, 2019.

[17] M. Barhoumi, "The Density Functional Theory and Beyond: Example and Applications," pp. 1-3, 2021 DOI: 10.5772/intechopen.100618.

[18] P. Giannozzi, "An introduction to the plane-wave pseudopotential method," Universit`a di Udine and CNR-IOM Democritos, Trieste, Italy, 2020.

[19] Qimen Xu et al., "SPARC: Simulation Package for Ab-initio Real-space Calculations," *SoftwareX,* vol. 15, pp. 3-4, 2021.

[20] Xavier Blase, "Introduction to Density Functional Theory," Institut Neel, CNRS, Grenoble, France, 2017.

[21] G. Colò, "Nuclear density functional theory," *Advances in Physics: X,* vol. 5, no. 1, pp. 1-2, 2020, DOI: 10.1080/23746149.2020.1740061.

[22] Klaus Capelle, "A Bird's-Eye View of Density-Functional Theory," *Brazilian Journal of Physics,* vol. 36, no. 4A, pp. 1-2, 2006.

[23] Trygue Helgaker, "Density-functional theory," Centre for Theoretical and Computational Chemistry, University of Oslo, Norway, 2008.

[24] C. Pal, "Design and Optimization of Lattice Structure: A Review," School of Mechanical Engineering, Beijing Institute of Technology, China, 2020.

[25] K. Sharkas, "Double-hybrid density-functional theory made rigorous," *The Journal of Chemical Physics,* vol. 134, no. 6, pp. 6-7, 2011 doi: 10.1063/1.3544215.

[26] C. Stampf and C. G. Van de Walle, "Density-functional calculations for III-V nitrides using the local-density approximation and the generalized gradient approximation," *PHYSICAL REVIEW B,* vol. 59, no. 8, pp. 3-7, 1999 doi:10.1103/physrevb.59.5521 .

